International Conference on Space Optics—ICSO 2014

La Caleta, Tenerife, Canary Islands

7–10 October 2014

Edited by Zoran Sodnik, Bruno Cugny, and Nikos Karafolas

From the optical characteristics of Herschel-hifi to in-orbit spatial response calibration using Mars

W. Jellema

D. Doyle

International Conference on Space Optics — ICSO 2014, edited by Zoran Sodnik, Nikos Karafolas, Bruno Cugny, Proc. of SPIE Vol. 10563, 105633E · © 2014 ESA and CNES
CCC code: 0277-786X/17/$18 · doi: 10.1117/12.2304199

FROM THE OPTICAL CHARACTERISTICS OF HERSCHEL-HIFI TO IN-ORBIT SPATIAL RESPONSE CALIBRATION USING MARS

W. Jellema[1,2] and D. Doyle[3]
[1]*SRON Netherlands Institute for Space Research, P.O. Box 800, 9700 AV, Groningen, the Netherlands,*
[2]*Kapteyn Astronomical Institute, P.O. Box 800, 9700 AV, Groningen, the Netherlands,*
[3]*ESTEC, Optics Section (TEC-MMO), Keplerlaan 1, P.O. Box 299, 2200 AG, Noordwijk, the Netherlands.*

ABSTRACT

Making use of all Mars observations taken by Herschel-HIFI, we present a detailed comparison of the measured and predicted beam profiles observed in space. Starting with a number of instrument beam profile models, including one based on actual wavefront measurements in the 480 – 1625 GHz frequency range, we developed a forward model predicting the detailed characteristics of the beam profile at the sky. Once convolved with the actual brightness temperature distribution and appearance of Mars, this forward model can be compared in detail with the observed spatial response towards Mars, using the science data of HIFI. Since the HIFI instrument is a single-mode coherent receiver, and given the availability of phase-sensitive measurements at instrument level, the results suggest that it is possible to extract some interesting optical characteristics of the Herschel telescope in addition. We discuss a possible way to extract the location of the telescope focus from these observations, which could provide useful feedback to the thermo-elastic properties of the SiC telescope assembly under zero-g and cryogenic conditions.

I. INTRODUCTION

The Heterodyne Instrument for the Far-Infrared (HIFI) was one of the three instruments onboard the Herschel Space Observatory [1], which was launched into space in May 2009, and successfully operated until it was switched off in June 2013. With the data collected by Herschel, many new discoveries in the field of far-infrared and sub-millimeter wave astronomy have meanwhile been made, and astronomers continue to report significant results contributing to our understanding of the formation and evolution of galaxies in the early Universe, chemical composition of solar system objects, and star formation and molecular chemistry of the Universe.

Benefitting from the largest single mirror ever built for a space telescope [2], Herschel-HIFI was a heterodyne spectrometer hunting for the spectral signatures of molecules by means of unprecedented spectral resolution at nearly quantum-limited performance [3]. By virtue of its high spectral resolution HIFI was particularly well suited to probe the physical conditions and chemistry involved in the processes referred to above. HIFI was a single pixel instrument offering continuous spectral coverage across the 480-1250 and 1419-1910 GHz bands. The instrument was divided up into 7 mixer bands, where only one band was active at a given time, operating on orthogonal polarizations received by two independent mixers. An illustration of the Focal Plane Unit (FPU) of HIFI is given in Fig. 1.

HIFI was and is still aiming at an absolute calibration accuracy of 10%, with a goal of 3%. For this reason the HIFI Instrument Control Center (ICC), currently in the post-operation phase, is still heavily working on improving and updating the calibration of HIFI in a final attempt to leave behind the best possible legacy archive. The associated calibration activities make use of an enormous scientific archive built up over 4 years of mission lifetime, as well as engineering data collected in the form of housekeeping data and measurements taken during ground and pre-launch testing.

One of the components of the post-calibration activities for HIFI concerns the calibration of the spatial response. Only very recently the detailed beam patterns were derived from the combined analysis of all observations presently available in the archive. Although very sensitive in terms of taking very high resolution spectra, HIFI suffered from intrinsically limited continuum or photometric sensitivity, and together with the single-pixel nature of the instrument it turned out to be very expensive to take high signal-to-noise beam maps with sufficient spatial extent and sampling. Only by combining all suitable observations at the end of the mission we could build up the desired signal-to-noise, or effective integration time, and spatial sampling of the patterns.

In this paper we briefly summarize the spatial response calibration procedure by reviewing some of the theory and methods used. We present a forward model, by assuming electromagnetic reciprocity, and treating the mixer horns as transmitters, yielding beam patterns at the sky. Once convolved with the actual source brightness temperature distribution, this model can be used to calculate the absorbed power in receiving mode, expressed as an antenna temperature. Referenced against the internal radiometric calibration loads this allows us to determine several system efficiencies, which are closely related to the optical properties of the end-to-end signal chain. Interpreting the results obtained we find indications of possible wavefront errors currently not accounted for. Although these errors do not matter to first-order, the quality of the data, the outstanding stability and reproducibility observed during the mission, now allow us for the first time to potentially refine our knowledge of some optical engineering quantities, perhaps even to second-order. We therefore propose and discuss a

possible way to extract these properties, as applicable in space under cryogenic and zero-g conditions, by combining the scientific calibration and optical engineering data obtained during ground measurements. This potentially opens up the possibility to further refine our knowledge of the position of the telescope focus in orbit, the absolute magnitude of the dominant aberrations of the telescope, which could provide useful feedback to the thermo-elastic properties and design of the SiC telescope assembly.

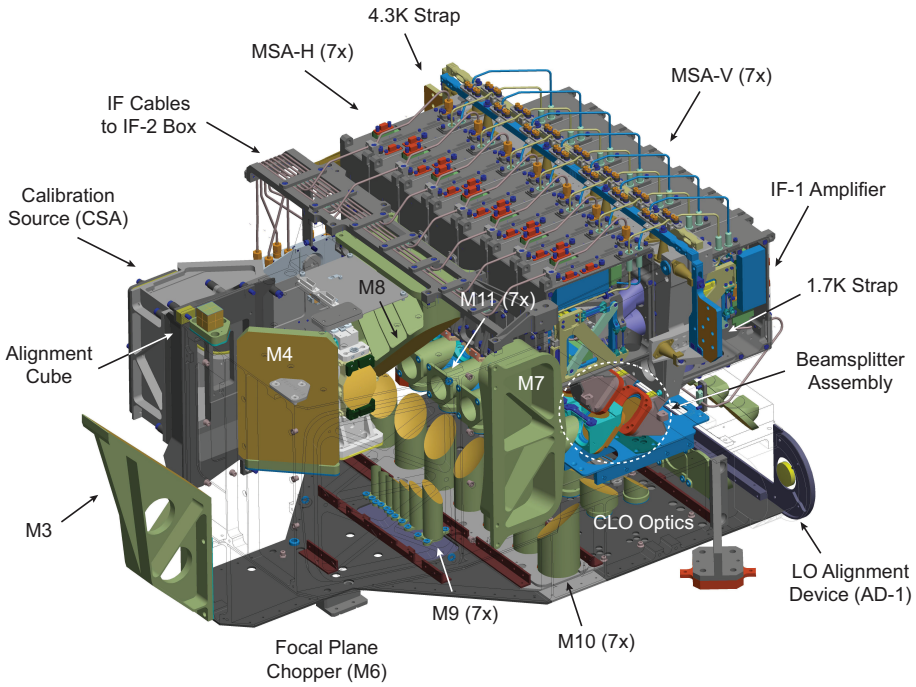

Fig. 1. Inside view on the optics of the FPU of HIFI. An Offner relay re-images the telescope focal plane, picked-off by mirror M3, to a row of 7 individual field mirrors dividing the HIFI Field-of-View (FoV) into seven mixer pixels.

II. CALIBRATION OF THE SPATIAL RESPONSE OF HIFI

A. Objectives

The primary objective of the spatial response calibration activity was to extract the detailed normalized beam profile $P_n(\theta,\phi)$ of each aperture of HIFI from all suitable observations taken to date. By having detailed knowledge of the beam profiles it becomes possible to calibrate the spatial response of HIFI to arbitrary source distributions. In the end we wanted to obtain a calibrated relation between the source brightness temperature distribution $T_b(\theta,\phi)$ and the observed antenna temperature $T_a(\theta,\phi)$. The source brightness temperature distribution is expressed in terms of its equivalent Rayleigh-Jeans temperature. The antenna temperature defines the power received as $P = k_B T_a \Delta\nu$, where k_B denotes Boltzmann's constant, and $\Delta\nu$ the spectral bandwidth of interest.

B. Calibration observations

In order to realize sufficient signal-to-noise, only relatively strong sources, with known spatial distribution, were selected. This limited the range of objects to planets and point sources with strong line emission. We decided as a first step to constrain the dataset to all Dual-Beam Switched (DBS) maps taken towards Mars. Mars was observed a number of times during the mission, basically every time it became visible on the sky. It was observed at a relatively large number of spot frequencies evenly distributed across the HIFI spectral range, as part of routine periodic engineering observations. Excellent models of the spatial distribution of Mars as function of time, at which the planet appeared during the different epochs, were made available by Raphael Moreno. The model is available at http://www.lesia.obspm.fr/perso/emmanuel-lellouch/mars/. At some frequencies Mars was observed during four different epochs. The apparent size of Mars varied from 5.3" up to 9.3". The nominal Full Width at Half Maximum (FWHM) of the HIFI beams varied between 11" in band 7, and 43" in band 1. Although Mars was certainly not resolved by HIFI, we could neither ignore the extended nature of the planet relative to the HIFI beam width, hence the spatial maps of Mars were key to our analysis. In order to keep the total observing time, dedicated to these calibration observations, within reasonable

limits, the maps towards Mars were relative coarse and small. Typical maps were square Nyquist sampled maps containing 7x7 spatial samples. In the second half of the mission we switched however to higher spatial sampling, varying between FWHM/4 and FWHM/3, in a striped pattern of 3x20 samples, which were mutually crossed and interlaced to achieve good main beam sampling, whereas the 1st diffraction ring could also be captured. Although individual maps did not have particularly good sampling and spatial extent, combining and cascading all observations at a given frequency did give very good spatial sampling and coverage, as different observations were taken with different relative orientation and sampling geometries.

C. Theory

The observed antenna temperature across a DBS raster map taken towards Mars can be described by the following equation [4]:

$$T_a(\theta,\phi) = \left(\frac{A_e}{\lambda^2}\right) \iint T_b(\theta'-\theta,\phi'-\phi)\, P_n(\theta',\phi') d\Omega'. \quad (1)$$

Equation (1) states that the observed antenna temperature is the convolution of the spatial distribution of the source and the normalized beam pattern. The effective collecting area A_e equals $\eta_a A_g$, where η_a denotes the aperture efficiency of the instrument, and A_g the geometrical area of the unobscured entrance pupil of the telescope. Once the normalized beam pattern $P_n(\theta,\phi)$ is known, and the aperture efficiency η_a, the calibrated spatial response to arbitrary source distributions can be calculated.

Defining the source solid angle Ω_s as

$$\Omega_s = \iint \psi\,(\theta',\phi') d\Omega', \quad (2)$$

where $\psi(\theta,\phi)$ is the normalized source distribution function, a beam-weighted source solid angle Ω_Σ can be defined as follows:

$$\Omega_\Sigma = \iint P_n(\theta',\phi')\psi\,(\theta',\phi') d\Omega'. \quad (3)$$

Using the antenna theorem [4] and after some algebra it can be shown that (1) can be rewritten to obtain an explicit relation for the aperture efficiency η_a:

$$\eta_a = \left(\frac{2k_B}{A_g}\right)\left(\frac{T_a}{S_\nu^{tot}}\right)\frac{\Omega_s}{\Omega_\Sigma}. \quad (4)$$

Equation (4) states that the aperture efficiency equals the product of the nominal Kelvin to Jansky conversion factor $(2k_B)/A_g$ of the telescope, the ratio between the peak antenna temperature T_a observed and the total source flux S_ν^{tot} incident on the telescope, and finally the ratio of the source and beam-weighted source solid angles defined in (2) and (3). The recipe to obtain the aperture efficiency is contained in these equations and requires the following steps:

- Measure $T_a(\theta,\phi)$ towards Mars
- Fit a beam model $P_n(\theta,\phi)$ convolved with Mars to the measured response
- Extract the peak antenna temperature T_a
- Calculate the total source flux S_ν^{tot} incident on the telescope
- Evaluate the dilution factor Ω_s/Ω_Σ using P_n and the Mars distribution

A similar relation can be derived for the main beam efficiency. The main beam efficiency is the fraction of power that is contained in the main beam. The main beam semi-angle is defined by the first inflection point of the Encircled Energy Fraction (EEF) diagram of the beam pattern, which corresponds to the angular radius of the first dark ring of the diffraction pattern. The main beam efficiency can be expressed as

$$\eta_{mb} = \frac{\Omega_{mb}}{\Omega_a}, \quad (5)$$

where Ω_{mb} is the main beam solid angle and Ω_a the entire antenna solid angle. Using (1) it can be shown that (5) can be written as:

$$\eta_{mb} = \left(\frac{T_a}{T_b(0,0)}\right)\frac{\Omega_{mb}}{\Omega_\Sigma} \overset{\text{def}}{=} \frac{T_a}{T_{mb}}. \quad (6)$$

In this equation T_a represents the peak antenna temperature observed, and $T_b(0,0)$ denotes the reference brightness temperature used in the normalization of $\psi(\theta,\phi)$. Equation (6) also implicitly defines a main beam

temperature. There is however a completely independent relation, which can be obtained by applying the antenna theorem, and which links the main beam efficiency to the aperture efficiency simply by having detailed knowledge about the beam pattern:

$$\eta_{mb} = \eta_a \frac{A_g \Omega_{mb}}{\lambda^2}. \quad (7)$$

D. Forward beam model

The forward model, referred to in the introduction, starts with the initial assumption that the beams of individual mixer pixels in the focal plane can be reasonably well represented by a simple Gaussian without aberrations. The beam width of this Gaussian is a free parameter. This beam is then propagated forward through a telescope model based on the as-built flight configuration. The telescope model includes the WFE predicted for flight by the telescope manufacturer, as well as the detailed obscuration by the support structures of the secondary mirror M2. Depending on the beam parameters of the Gaussian, the field level at which the beam is truncated at the secondary mirror, the so-called edge taper, can be varied. The beam truncation is parameterized by α, which is related to Gaussian beam waist radius w_0 in the focal plane by

$$w_0 = \frac{2}{\pi}\sqrt{\alpha}\lambda F, \quad (7)$$

where F is the focal ratio of the telescope, which equals 8.68 for Herschel. The edge taper T_e is the relative intensity level of the Gaussian, measured at the edge of the secondary mirror of the telescope, expressed in decibel. The edge taper T_e is also related to the beam truncation parameter α by the following equation:

$$T_e = \frac{20\alpha}{\ln(10)}. \quad (8)$$

For a given edge taper value, the forward model translates into a complex field distribution across the aperture plane of the telescope, which is subsequently Fourier transformed into a far-field radiation pattern. Applying electromagnetic reciprocit, it can be shown that this pattern is identical to the reception pattern, or PSF, of the HIFI instrument.

The model is generic; it is therefore possible to assume a different input field distribution. The model can propagate an arbitrary complex field distribution in the focal plane through the telescope. An example assuming a measured complex field distribution during Instrument Level Testing (ILT) is given in Section III.C.

D. Analysis procedure

Using the forward model described in the previous section, a numerical analysis procedure was carried out. As a first step all observations towards Mars were sorted by frequency, mixer band and polarization. Observations taken within a few GHz around the same frequency were clustered. For each observation a Mars model was generated applicable at the time of the observation. Next a three-dimensional data cube was generated for each observation. Each frame, or two-dimensional image, in this data cube represented a beam model at a particular edge taper value, which was varied across the third dimension of the cube. Since the appearance and distribution of the source was deterministic, each frame was subsequently convolved with the spatial map of Mars. This pre-calculated data cube was used by an interpolation routine yielding the amplitude of the convolved beam model as function of θ, ϕ and T_e.

As a second step a non-linear least-squares minimization procedure was executed, fitting an optimal value of T_e matching all observations around the frequency of interest, or within a particular mixer band, assuming the as-designed wavelength independence of T_e. The pointing offset was removed in each individual observation, and in addition to T_e, the amplitude was also fitted to obtain the observed peak antenna temperature T_a.

Finally a post-processing routine tabulated and plotted a set of relevant beam properties, as well as the aperture and main beam efficiency, for each individual observation in the data set. It is noted that there are two independent estimates of the efficiencies possible. The primary one is based on a top-down approach using (4) and (6), and the science data, where the T_a scale of the observations is calibrated against the internal radiometric loads. It is however also possible to calculate the efficiencies without using the observed peak antenna temperature, after fitting a beam model to the normalized beam pattern, in a bottom-up approach entirely based on the model fit. The aperture efficiency simply follows from a field overlap integral in the telescope aperture [4], after which the main beam efficiency can be calculated using (7), or by using the detailed beam pattern, and keeping proper track of the spillover and blockage losses. Ideally the solution is self-consistent, meaning that if the instrument beam is sufficiently well represented by a simple Gaussian, and if the telescope model is valid, top-down (science data) and bottom-up (model fit) estimates should be identical.

III. DISCUSSION OF RESULTS

A. Gaussian beam model

In Fig. 2 we show a typical result obtained for a specific observation in mixer band 6H (where H stands for Horizontal polarization) part of a clustered dataset around 1625 GHz. The peak antenna temperature is about 37 K, and the rms residual of the fit equals 0.4 K, which is very close to the rms noise of this detector. In the left panel linear cuts on a logarithmic scale are shown across a 3x20-striped pattern in comparison to the convolved model fit. At the right hand side a typical 7x7 raster map is shown during another observation in the same band. At the top the measurement (left) and the model fit (right) are shown, at the bottom the residuals (left) and the unconvolved beam model (right) with respect to the telescope coordinate system. The model captures all details quite well. In addition to a good match of the FWHM, the asymmetric sidelobe structure and diffraction rings are accurately described, and the triangular inner core and beam shape due to telescope trefoil can be clearly recognized.

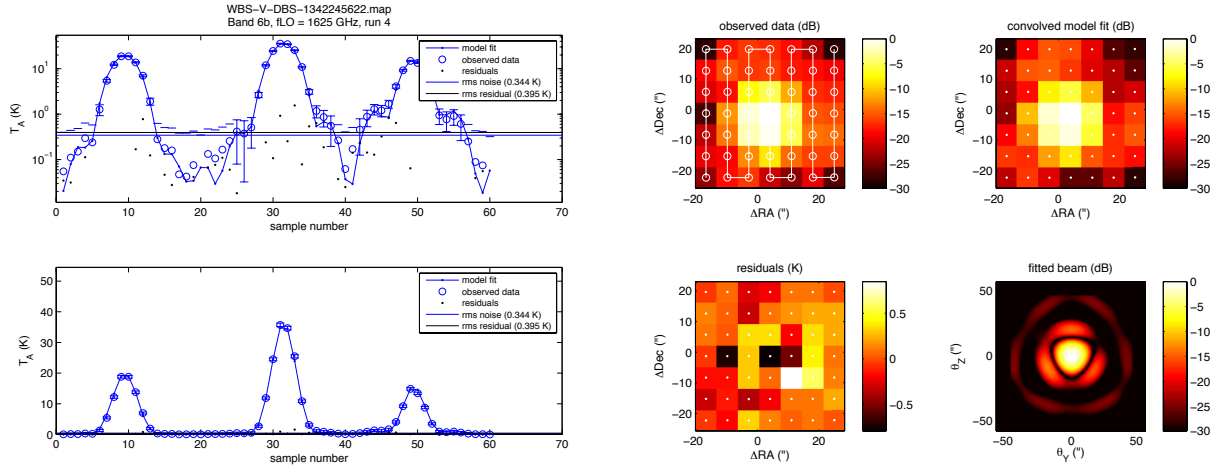

Fig. 2. Examples of observed antenna temperature profiles in comparison to forward model fits in band 6H at 1625 GHz.

Next we show the fitted edge taper values of the beam models in comparison to the expected values determined during ILT in the left-hand panel of Fig. 3. The data are plotted in sequence of aperture number, starting with 1H, 1V, 2H, … 7H, and ending with 7V. The average value over all apertures is 10.3 ± 1.3 dB, which is slightly smaller than the expected average of 10.7 ± 1.5 dB. The FWHM is however not very sensitive to the exact value of the edge taper, and both results agree within the error bars. Note that the design value for HIFI was 10.9 dB. Differentiation between mixer types shows however an interesting difference. At lower frequencies in bands 1 to 4, corrugated horns were used producing highly Gaussian beams, whereas at higher frequencies in bands 5 to 7, integrated lens-antennas were used with lower Gaussicity. Looking only at the corrugated horn bands, the average observed edge taper equals 9.8 ± 0.7 dB, whereas we should have seen 11.2 ± 0.5 dB based on ILT results. The error bars of these averages do not overlap, and suggest that for these mixer bands there is a systematic deviation of -1.4 dB in edge taper. For the higher frequency bands the picture is mixed or even opposite. Band 5 seems to be an outlier with respect to the general trend.

This is also seen when we plot the observed efficiencies vs. frequency in the right-hand panel of Fig. 3. The general trend shows decreasing efficiency with increasing frequency. This trend is however broken by band 5, which is clearly an outlier and which will be further addressed in Section III.C. Comparing the top-down (science data) and bottom-up (model fit) derived efficiencies, it is clear that we find self-consistent solutions within 1-2% for the majority of the bands, whereas for particular bands larger discrepancies (up to 4-6%) are observed, specifically in band 5 (aperture numbers 9 and 10). The outliers support the idea that the Gaussian approximation might not be completely valid everywhere. In the efficiency plots we also show fits (excluding band 5) to the general trends using Ruze's equation [5]:

$$\eta(\lambda) = \eta_0 \exp\left[-\left(\frac{4\pi\delta}{\lambda}\right)^2\right]. \tag{8}$$

In (8) η either represents the aperture or the main beam efficiency. Equation (8) is very similar to the well-known behaviour of the Strehl ratio with respect to wavelength in the presence of wavefront errors. The general trend observed is consistent with an rms WFE (= 2δ) of 8.2 ± 0.4 μm. Earlier in the mission, using a smaller data set, we found a value of 7.6 ± 1.8 μm. The SPIRE instrument on Herschel also had to scale the predicted

WFE of the telescope up by about 50% in order to match their measured beam profiles. These independent observations suggest that the telescope WFE could be about 1.5 to 2 times larger than predicted for flight, or a misalignment (defocus) somewhere in the end-to-end system.

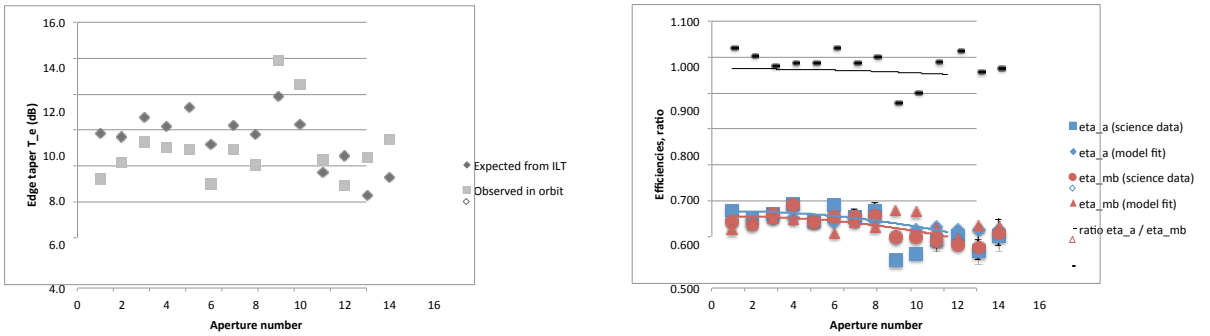

Fig. 3. Fitted edge taper values (left) and (ratio of) efficiencies (right) for all apertures of HIFI. For reference the expected ILT edge taper values (left) and ratio of aperture and main beam efficiency at the design value of 10.9 dB are also shown. The solid efficiency curves in the right-hand figure represent fits to Ruze's equation excluding the data for band 5.

B. Observed issues and discrepancies

Possible systematic deviations in edge taper, deviations between top-down (science) and bottom-up (model) estimates of the efficiencies, and in particular the apparent magnitude of the rms WFE, all clearly indicate that a simple Gaussian beam model ignoring the intrinsic instrument and telescope aberrations might not be accurate enough to describe the optical system properties to 2nd order. There is a clear need to account for the actual wavefronts of the instrument incident on the telescope, and to review the absolute magnitude of the telescope aberrations in orbit. Whereas some of the observed characteristics could be waived away by the approximations in the model, the general trend of the observed efficiencies is real, based on accurate radiometric science data, which is not very sensitive to 2nd order details of the beam model. This means that the excess WFE could actually be real. This hints into the direction that one of the dominant aberrations is larger than expected or a misalignment (defocus). The obvious candidate is spherical aberration, which was not included in the telescope WFE map and flight performance predictions. In the next section we show how uncertainties in the instrument beam model can be disentangled by using actual ILT data instead of a simple Gaussian approximation.

C. ILT wavefront data

In order to assess the feasibility of using ILT wavefront data to model the HIFI beam, we requested a special calibration observation near the end of the mission. Band 2H was selected considering signal-to-noise towards Mars. We observed Mars at 770 GHz across an extended 20x20 raster map. Sampling and spatial extent was adjusted to capture both inner details of the core and detailed features of the first diffraction ring.

We then went back to the ILT data taken on the ground. From the test archive we retrieved the phase and amplitude data of a field map taken at about 500 mm above the focal plane. The signal-to-noise ratio of this measurement was beyond 60 dB, and the absolute measurement geometry was known within fractions of a millimetre. Since we measured the phase of the electric field distribution directly, by using heterodyne antenna measurement techniques [6], we could propagate the measured field to the secondary mirror M2 (pupil) of the telescope. The reconstructed intensity and phase distribution at M2 is shown in Fig. 4. A dotted circle indicates the edge of M2. The phase is referenced to the as-designed wavefront of the telescope. From Fig. 4 it can be seen that we now properly take into account the instrument aberrations (there is some coma and spherical aberration). Considering the total system WFE, including the flight prediction for the telescope scaled up by a factor of 1.5, we find a rms WFE of 6.4 μm (geometrical) and 5.4 μm (intensity weighted), which is still smaller than the observed value determined from the in-orbit efficiencies (see Section III.A).

In Fig. 5 we show the convolved beam pattern and linear crosscuts of the far-field pattern. Note the asymmetry of the inner core, and in the first sidelobes, due to dominant trefoil of the telescope. The peak sidelobe level, measured on the first diffraction ring, equals -16.2 dB, which can easily be detected by HIFI. Figure 6 compares the modelled and observed beam pattern. The agreement between model and the calibration observation is remarkable. The main beam distortions, asymmetries and overall structure are generally reproduced to within the noise of the measurement, with the exception of some very localized and low amplitude (2-3 sigma) systematic residuals. This comparison clearly confirms the potential of using the ILT wavefronts for beam modelling.

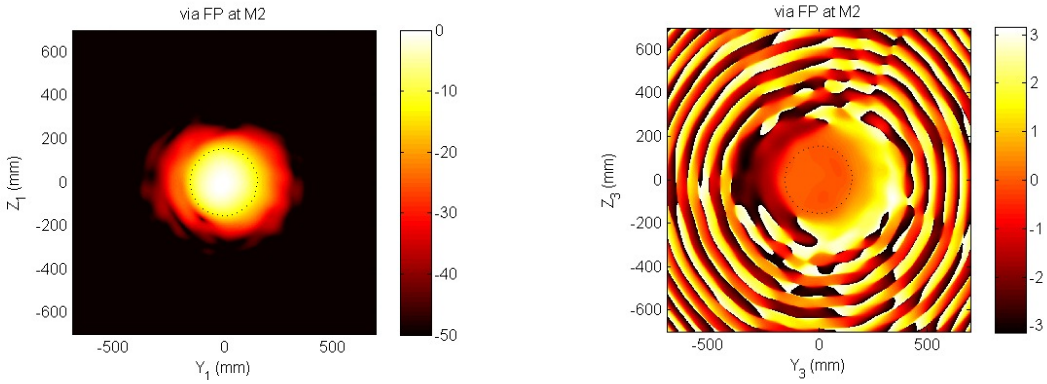

Fig. 4. Phase sensitive ILT beam measurement of band 2H propagated to the M2 pupil plane.

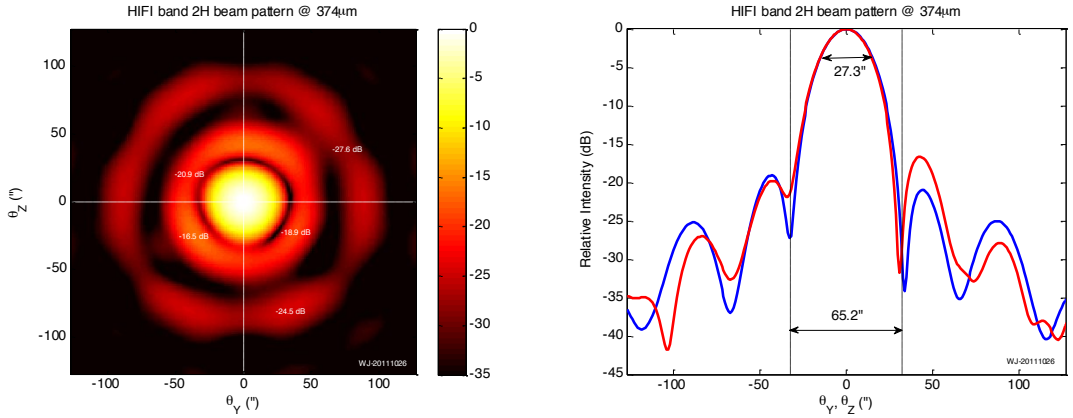

Fig. 5. Model prediction of the HIFI beam pattern of band 2H convolved with Mars assuming ILT data.

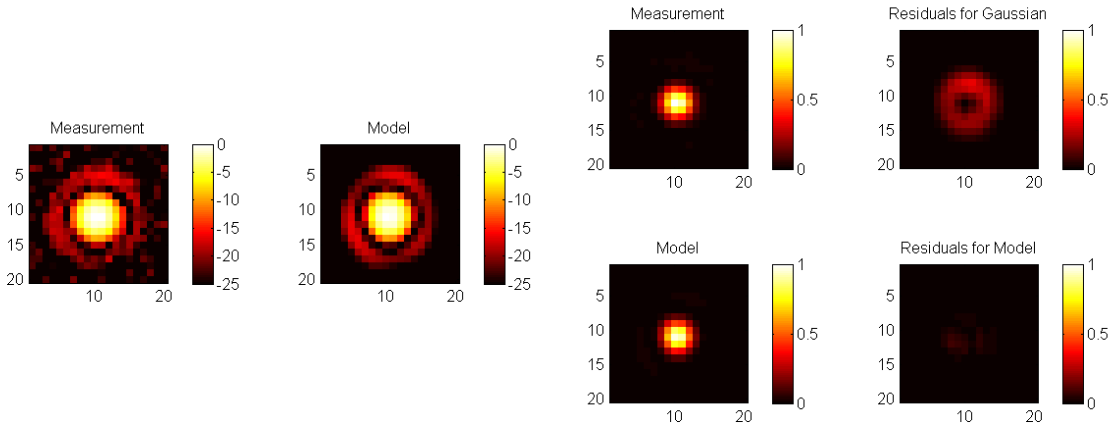

Fig. 6. Comparison of observed and modeled beam patterns towards Mars for HIFI band 2H.

Finally we compare the observed and modelled efficiencies. The observed aperture and main beam efficiency equals 66.3 ± 0.7% and 66.3 ± 0.7% resp. The ratio equals 1.00 ± 0.01. From the modelling we obtain 65.4% and 66.0% resp., and a ratio of 0.99. These results are in excellent agreement showing that model and measurement agree within 1%.

The same procedure was followed to investigate the outliers in band 5 from a modelling point of view. The model predicts that we should observe 12% lower aperture efficiency due to a combined effect of non-Gaussian illumination of M2 (power is more concentrated on the central hole in M1), a larger instrument WFE, and a lower spillover efficiency (larger amount of power outside of edge of M2). This is in good quantitative agreement with the observed drop in aperture efficiency, which equals 1 – (0.562 / 0.651) = 13.7%. Again this observation highlights that actual ILT wavefronts are probably the best inputs for the forward beam modelling.

IV. PROPOSED METHOD TO CONSTRAIN TELESCOPE FOCUS AND WFE

The results presented in Section III provide strong evidence that phase sensitive beam measurements of the HIFI flight instrument are of key importance to constrain some optical system properties as observed in space. With the clear indication of some excess end-to-end WFE we propose a sensitive method to identify the root cause of these final 2nd order deviations, for system performances that are already excellent and confirmed to 1st order. We propose to simultaneously fit forward models, based on IL data, of all 14 apertures of HIFI to all observations taken to date towards Mars, and possibly other suitable planets. Constrained bottom-up by very accurate and phase-sensitive wavefront measurements with known absolute coordinates, and top-down by accurate radiometric calibration of aperture and main beam efficiencies, we will try to determine or constrain the amplitudes of the low-order Zernike terms of the telescope WFE, and investigate the location of the telescope focus in orbit. In Fig. 7 we show a preliminary model result for a Gaussian beam at 157 μm, assuming spherical aberration of the telescope, expressed as defocus of the system. Whereas the relative change of the FWHM, or main-beam angle, is insensitive to defocus, the relative change of the ratio between aperture and main-beam efficiency varies more rapidly with defocus. The FWHM can typically only be determined within 5-10% accuracy, whereas we belief that the ratio of aperture and main beam efficiencies can be determined within 0.1% accuracy. This will allow us, provided we get all sign conventions right, to refine our knowledge of the telescope focus potentially to within a few mm. Finally we belief that this method can also constrain the absolute magnitude of the dominant aberrations of the Herschel telescope. This information might eventually be of interest to the telescope manufacturer for evaluation of the thermo-elastic properties of SiC under cryogenic and zero-g conditions in space.

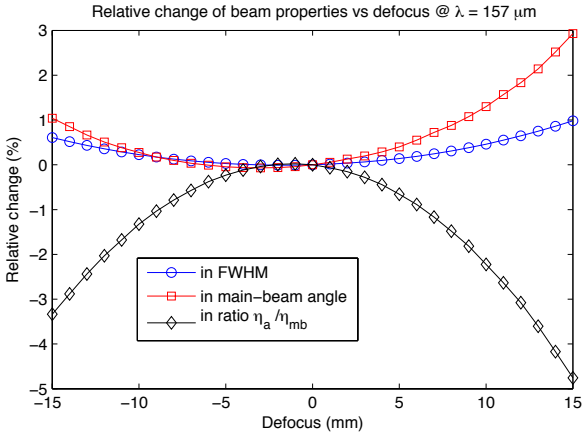

Fig. 7. Relative change of FWHM, main beam angle and ratio between aperture and main beam efficiency at 157 μm.

I. SUMMARY AND CONCLUSION

In this paper we show how spatial response calibration data obtained for Herschel-HIFI leads to the conclusion that there might be some excess system WFE currently not accounted for. We demonstrate how accurate and phase sensitive beam measurements taken at HIFI instrument level could be used to further constrain this 2nd order calibration issue. We finally propose a potentially very accurate method, employing radiometric calibration data and optical test data of HIFI, that could further refine our knowledge of the Herschel telescope focus, as well as other system WFE components applicable at telescope and instrument level.

REFERENCES

[1] G. L. Pilbratt, J. R. Riedinger, T. Passvogel, G. Crone, D. Doyle, U. Gageur, A. M. Heras, C. Jewell, L. Metcalfe, S. Ott, and M. Schmidt, "Herschel Space Observatory. An ESA facility for far-infrared and submillimetre astronomy," *A&A*, 518:L1, July 2010.

[2] D. Doyle, G. Pilbratt, and J. Tauber, "The Herschel and Planck Space Telescopes," *IEEE Proceedings*, 97:1403–1411, August 2009.

[3] T. de Graauw et al, "The Herschel-Heterodyne Instrument for the Far-Infrared (HIFI)," *A&A*, 518:L6, July 2010.

[4] P. F. Goldsmith, *Quasioptical systems: Gaussian beam quasioptical propagation and applications*, IEEE Press, New York, 1998.

[5] J. Ruze, "Antenna Tolerance Theory – A Review," *IEEE Proceedings*, 54:633–642, April 1966.

[6] A. D. Yaghjian, "An overview of near-field antenna measurements," *IEEE Trans. A&P*, 34:30–45, January 1986.